Nanoscale

PAPER

View Article Online
View Journal | View Issue

Cite this: *Nanoscale*, 2026, **18**, 6399

Selective binding of sulphated glycosaminoglycans induces self-assembly of naphthalene diimide into fluorescent nanofibers

Poonam Sharma, [a,e] Esteban Fernández-Pedrera López,[a] Beatriz Cantero Nieto,[b] Annalisa Calò,[b,c,d] Subhadip Ghosh, [b] Paula Rodríguez,[a] Xavier Companyó, [a] Bart Limburg [a,e] and Mohit Kumar *[a,b,e]

The self-assembly of π-conjugated chromophores directed by biomolecular recognition offers a smart strategy to create bio-synthetic hybrid nanomaterials with emergent properties. Here, we report a novel amphiphilic, cationic naphthalene diimide (NDI) derivative that undergoes supramolecular polymerization upon interaction with anionic glycosaminoglycans (GAGs). Binding of GAGs like heparin to NDIs leads to their supramolecular polymerization in aqueous media. Interestingly, such binding events result in highly emissive fluorescent nanofibers due to the formation of a static excimer. Spectroscopic and microscopic investigations reveal that polyanionic heparin helps to bring the cationic NDIs into close proximity to promote π–π stacking and that amphiphilic self-assembly is essential for excimer formation. The heparin binding-induced excimer formation exhibits a clear emission color change from blue to bright green. Furthermore, the NDI selectively binds to sulphated GAGs such as heparin and chondroitin sulphate, but not to carboxylated hyaluronic acid, resulting in a differential fluorescence response. Thus, this study presents a heparin binding-induced supramolecular polymerization of a novel NDI derivative, providing a design strategy for controlling supramolecular order and for creating functional fluorescent nanomaterials for future biosensing and bioimaging applications.

Received 15th November 2025,
Accepted 28th January 2026

DOI: 10.1039/d5nr04833h

rsc.li/nanoscale

Introduction

Supramolecular organization of π-conjugated chromophores has emerged as a smart strategy to design functional nanomaterials with tunable optoelectronic, photophysical, and biologically relevant properties.[1] Such organizations are typically governed by a combination of noncovalent interactions, like π–π stacking, van der Waals forces, *etc.*, which are intrinsically encoded in the molecular design. In recent years, a complementary approach for self-assembly has emerged in which the binding of functional molecules with external chemical guests induces supramolecular ordering.[2] This has resulted in supramolecular polymers with unique properties like guest-induced chirality, chiral memory, stimuli responsiveness, *etc.*[1d,3] Additionally, when these guests are biomolecules, it opens up the possibility for (i) biomolecular recognition and (ii) developing bio-synthetic hybrid nanomaterials for various applications. In this regard, several molecules have been designed to self-assemble in the presence of bio-analytes, like nucleotides, amino acids, proteins, sugars, *etc.*[4] However, reports on the supramolecular polymerization of π-conjugated molecules in the presence of glycosaminoglycans (GAGs) like heparin remain scarce.[5] Additionally, controlling the fluorescent properties of supramolecular nanomaterials upon interaction with biomolecules is important to facilitate biotechnological applications. In this regard, GAG-triggered self-assembly resulting in fluorescent nanostructures remains unexplored, despite its clear potential for biosensing and bioimaging.

GAGs are anionic polysaccharides present in the extracellular matrix (ECM) of connective tissues, which provide functions like structural support, cellular communications, *etc.* Three major components of GAGs are heparin, chondroitin sulphate (CS) and hyaluronic acid (HA), of which the first two contain sulphated anions, whereas the last one contains only carboxylic acid groups as anionic groups. Among the three, heparin is extensively studied, is biologically present and is widely utilized as an anticoagulant drug. Therefore, significant effort has been devoted to developing heparin-responsive supramolecular materials. For example, peptide-based

[a]*Department of Inorganic and Organic Chemistry, University of Barcelona, Calle Marti i Fraquès 1-11, 08028 Barcelona, Spain. E-mail: mohit.kumar@ub.edu*
[b]*Institute for Bioengineering of Catalonia (IBEC), Calle Baldiri Reixac 10-12, 08028 Barcelona, Spain*
[c]*Department of Electronic and Biomedical Engineering, University of Barcelona, Calle Marti i Fraquès 1-11, 08028 Barcelona, Spain*
[d]*Institute of Nanoscience and Nanotechnology, University of Barcelona, 08028 Barcelona, Spain*
[e]*Institut de Química Teòrica i Computacional, University of Barcelona, 08028 Barcelona, Spain*

heparin-responsive nanomaterials have been used to regulate cellular growth.[6] The π-conjugated systems reported for heparin sensing are typically monomeric systems that do not form self-assembled nanostructures. In some cases where self-assembly occurs, the observed signals originate from the aggregates in which heparin remains unbound.[5a,7a–f] Several polymeric and small-molecule fluorescent probes have also been reported to detect heparin and other cellular microenvironments.[7g–i] Additionally, there are a few examples of heparin binding-induced supramolecular polymerization of pyrene and other π-conjugated chromophores,[5c,e,8] but arylenediimide derivatives are rarely reported.[5b,9]

Among π-conjugated molecules, arylenediimides like naphthalene diimide (NDI) and perylenediimide belong to an important class of organic semiconductors for application in sensing, (opto-)electronics, *etc.*[10] Since, self-assembly of arylenediimides is essential for various applications, the design of new GAG-directed systems that can control supramolecular ordering is needed. In this regard, here we present a novel example of heparin binding-induced self-assembly of NDI derivatives. Such NDI-based systems can produce novel biosynthetic functional nanomaterials. Furthermore, to the best of our knowledge, this is a unique example of heparin binding-induced formation of fluorescent nanostructures of any π-conjugated chromophores. Past reports have shown enhanced fluorescence in the presence of heparin in solution but not the formation of fluorescent aggregates.[5c,8b,11] The formation of fluorescent nanostructures is relevant for applications not only in sensing and electronics, but also for biorelevant application in *in vitro* and *in vivo* fluorescence imaging of the glycocalyx and ECM. Furthermore, the ability to obtain differential fluorescence signals from various GAGs will be advantageous for chemically selective bio-imaging of the ECM.

Here, we report a novel cationic NDI derivative **1** and its self-assembly in the presence of heparin and other GAGs (Scheme 1). The molecular design consists of an aromatic NDI core with a hydrophobic aliphatic chain on one side and a hydrophilic quaternary ammonium derivative on the other side. Thus, the molecule has an amphiphilic character to assist in self-assembly in aqueous media, and the cationic group facilitates interaction with anions like heparin. In the past, we and others have shown that quaternary ammonium groups can have strong interaction with sulphated anions.[12] Our previous work showed that heparin binding resulted in the induction of supramolecular chirality in the self-assembly of an achiral PDI derivative.[12b] We demonstrated heparin-assisted control over supramolecular ordering, but it caused complete quenching of fluorescence. On the other hand, in this work, we show that NDI derivative **1** efficiently binds to heparin to form an amphiphilic self-assembly that is highly fluorescent. Heparin binding-induced self-assembly results in the formation of a green-emissive excimer of **1**, which self-assembles into brightly fluorescent nanofibers. Thus, even though aggregation is known to quench the emission of fluorophores,[13] formation of an excimer from self-assembled **1** results in aggregation-induced green fluorescence. Furthermore, we demonstrate that **1** has strong affinity for sulphated GAGs and therefore it selectively binds to heparin and CS, and not to the carboxylated derivative HA, to form fluorescent nanofibers. This is advantageous as some of the previously reported fluorescent labelling methods for GAGs require covalent bond formation with saccharides, which cannot easily distinguish between various GAGs.[4c,14] Here, we show that **1** forms fluorescent nanostructures upon selective binding with heparin and CS, and thus can be potentially useful in fluorescent labelling to differentiate between GAGs. Using control molecule **2**, which is a bolaamphiphile, we established the essential role of amphiphilic design in the formation of excimers and fluorescent nanostructures. Thus, for the first time, we report (a) the heparin binding-induced formation of fluorescent nanofibers of any π-conjugated molecules and (b) sulphated GAG-directed self-assembly of an NDI derivative.

Results and discussion

Compound **1** was obtained by following a two-step synthetic procedure, as described in the SI (Scheme S1). Briefly, naphthalene-1,4,5,8-tetracarboxylic dianhydride was allowed to react simultaneously with decylamine and 1,1-dimethyl-

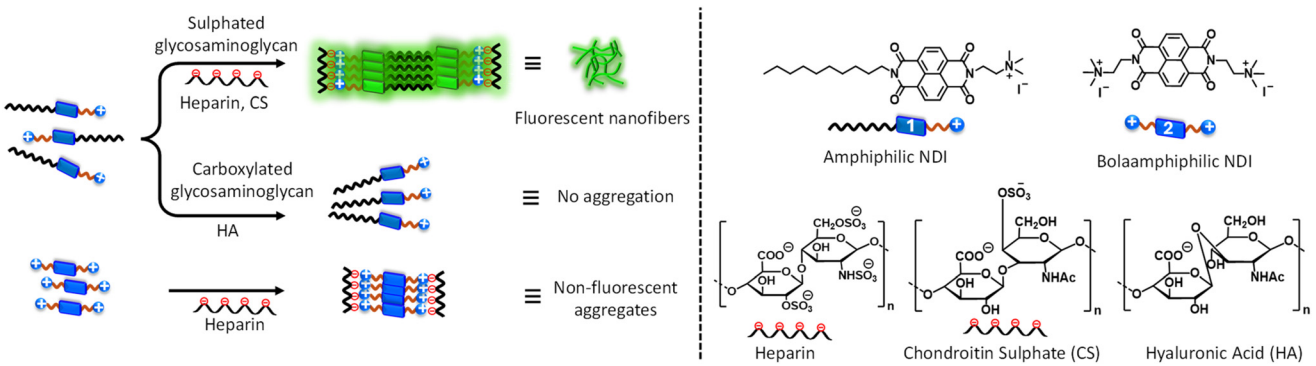

Scheme 1 Schematic of sulphated GAG binding-induced self-assembly and fluorescent nanofiber formation shown with the chemical structures of different molecules.

ethylenediamine to result in the desired NDI intermediate. This intermediate was methylated with methyl iodide to give **1** as a solid powder. Compound **2** was similarly synthesized (Scheme S2).

Solvent-dependent properties of compound 1

To gain insight into the self-assembly behavior of the amphiphilic molecule **1**, we first studied its photophysical behavior in varying solvent compositions of acetonitrile–H_2O. The compound was completely soluble in acetonitrile. The UV-Vis absorption spectra of a 50 μM solution in acetonitrile showed well-defined bands with maxima at 377 nm and 355 nm, corresponding to S_{0-0} and S_{0-1} vibronic peaks of NDI derivatives (Fig. S6a). These features clearly indicate the monomeric nature of **1** in acetonitrile. By increasing the % of water in acetonitrile from 0 to 99%, we expected to induce self-assembly of this amphiphilic molecule. Counterintuitively, we observed spectral features similar to those of monomeric NDI chromophores. To confirm the monomeric nature in the 99% water sample, we performed a temperature-dependent experiment. On increasing the temperature from 20 to 90 °C, no spectral change was observed, indicative of the monomeric nature of **1** (Fig. S6b). However, we did observe a 5 nm red shift of the absorption maxima from the 0% to the 99% water sample, which can be attributed to solvatochromic effects (Fig. S6a, c and d). This suggests that **1** mainly exists in the monomeric state in all the acetonitrile–water ratios and water is not able to induce self-assembly. To confirm the monomeric nature, we also recorded the ^{1}H NMR spectra of **1** in different solvent compositions. In acetonitrile, the NMR data showed a characteristic sharp aromatic peak of the naphthalene core at δ 8.67 ppm. Upon increasing the solvent polarity to 70 and 99% water, we observed no broadening of the NMR signal compared to the acetonitrile sample. The NMR results reestablish that **1** exists predominantly as a monomer (Fig. S7) in all acetonitrile–H_2O solvent compositions.

Heparin binding-induced supramolecular response

Heparin is an anionic biopolymer, so we investigated its potential electrostatic interaction with the cationic amphiphile **1** to induce self-assembly. Thus, we probed the interaction of the NDI derivative with heparin using UV-Vis absorption spectroscopy. First, samples of **1** with high water content (70% water in acetonitrile) were titrated with increasing amounts of heparin (Fig. 1a). We observed that the sharp monomeric absorption bands of **1** at 380 nm (S_{0-0}) and 360 nm (S_{0-1}) showed a gradual decrease in absorbance along with band broadening in the presence of heparin. Furthermore, the absorbance ratio at these two bands, S_{0-0}/S_{0-1}, changed from 1.23 to 0.89. This was accompanied by an increase in scattering and the appearance of an isosbestic point at 389 nm. These data clearly indicate interchromophoric π–π interaction, leading to the self-assembly of **1** upon binding with heparin in 70% water in acetonitrile.[15]

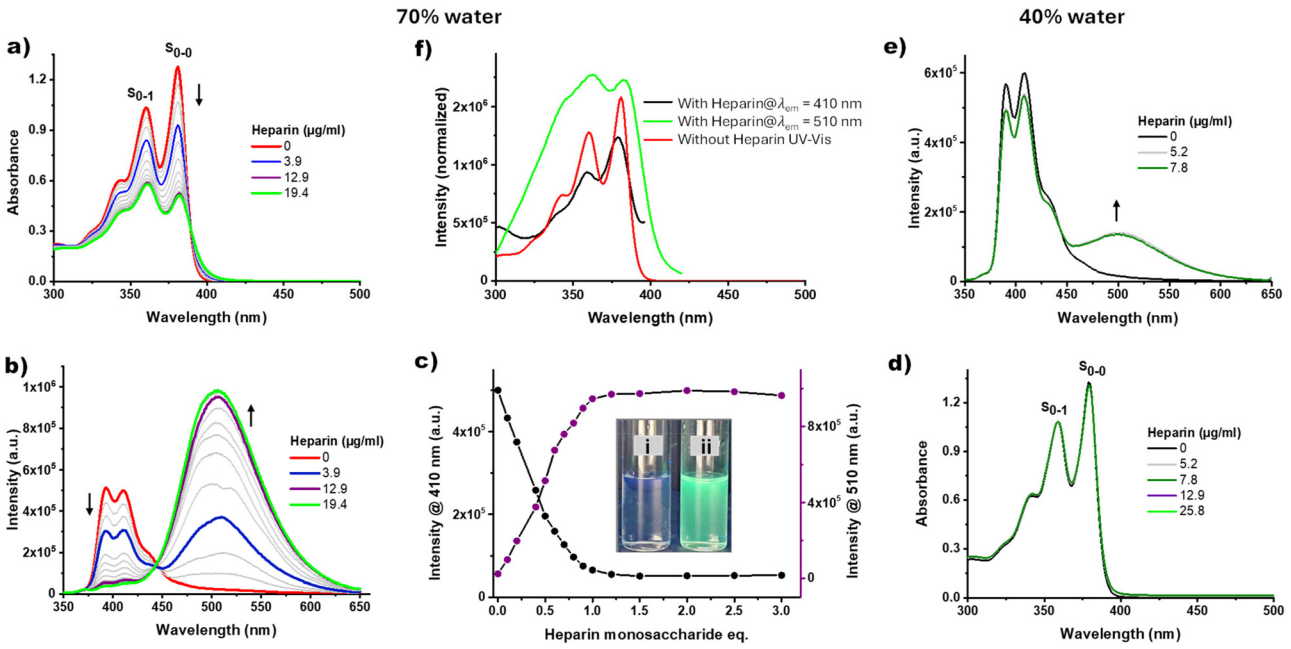

Fig. 1 (a) UV-Vis absorption and (b) emission spectra of **1** with varying concentrations of heparin in 70% water in acetonitrile solvent composition; (c) plot of emission changes of **1** at λ_{em} = 410 nm (monomeric emission) and 510 nm (excimeric emission) with different molar equivalents of heparin obtained from the data in (b). Heparin monosaccharide equivalents in (c) were calculated based on the monosaccharide concentration within polymeric heparin. Inset: photograph of a sample of **1** under 365 nm UV light in the absence (i) and presence (ii) of heparin; (d) UV-Vis absorption and (e) emission spectra of **1** with varying concentrations of heparin in 40% H_2O in acetonitrile solvent composition. (f) Excitation spectra collected at excimer and monomer emission at λ_{em} = 510 nm and λ_{em} = 410 nm, respectively, along with the absorption spectra of **1** alone in 70% H_2O in acetonitrile solvent composition. Concentration of **1** = 50 μM, λ_{ex} = 330 nm.

To gain further insight into heparin binding, fluorescence spectroscopy was used. The fluorescence spectra of **1** (without heparin) in 70% water showed monomeric features with maxima at 393 and 410 nm (λ_{ex} = 330 nm), as seen in Fig. 1b. The monomeric character was also confirmed by the excitation spectra collected at 410 nm. Interestingly, addition of heparin resulted in a significant decrease in the monomeric emission. This was accompanied by the appearance of a high-intensity emission band at 510 nm, which was broad and featureless and was approximately 100 nm red-shifted compared to the monomer (Fig. 1b). The supramolecular transformation from the monomer to the excimer was also confirmed by the appearance of an isoemissive point at 444 nm. Such broad emission at 510 nm has been assigned to the formation of an excimer in NDI derivatives.[16] These fluorescence color changes from blue (without heparin) to green (with heparin) can be easily observed under 365 nm illumination, as seen in the photograph (70% water in acetonitrile, Fig. 1c, inset). Furthermore, a plot of emission intensity at 510 nm against the equivalents of monosaccharide units of polymeric heparin demonstrates saturation at approximately 1 molar equivalent (Fig. 1c). Considering that each monosaccharide unit of heparin has approximately 1 anionic sulphation unit available for binding, this indicates a very efficient 1 : 1 interaction between **1** and heparin. Similar spectroscopic changes were also observed at higher water contents like 90 and 99% water in acetonitrile (Fig. S9a–d). These data confirm that at high water %, heparin binding induces supramolecular organization of **1**, facilitated by π–π interactions and hydrophobic effects, resulting in the formation of a highly emissive NDI excimer. Also, the UV-Vis and emission spectra of the drop-cast and dried film of **1** with heparin showed similar features of aggregated NDI and excimeric emission. This indicates that the solution-state self-assembly can be transferred to the solid dried film (Fig. S8a–b). Thus, we demonstrate that excimer emission upon heparin binding in **1** overcomes the aggregation-induced quenching effects of chromophores. Thus, this can be an alternative approach to obtain aggregation-induced emission in NDI derivatives.[13]

Next, we probed the effect of heparin binding in low water % solvent compositions. In these cases, the amphiphilic **1** will have a lower tendency to self-assemble. As expected, the monomeric absorption spectra of **1** alone in 40% water in acetonitrile did not show any significant change upon binding with heparin (Fig. 1d). This indicates that there is no significant binding of heparin to **1** to induce aggregation of NDIs in 40% water. The fluorescence spectra of **1** in the presence of heparin showed a minor decrease in the monomeric emission of **1** (391 nm and 409 nm), confirming that **1** remains mainly in its monomeric state. However, a low-intensity, red-shifted excimer emission at 500 nm (Fig. 1e) was also observed. Thus, the weak excimer formation upon heparin addition indicates that a small % of **1** indeed binds to heparin to induce aggregation. The fraction of **1** bound to heparin was estimated to be (≈7%), as obtained from the decrease in the monomeric emission in Fig. 1e. Similar observations were made with the 10% water in acetonitrile sample (Fig. S10a and b). These data confirm that at a low percentage of water, the self-assembly propensity and the heparin-binding efficiency of **1** are very low. Taken together, this implies a two-way process, *i.e.*, heparin binding induces aggregation of **1** (*e.g.*, in 70% water) and heparin binding is weak if it is not assisted by the tendency of **1** to self-assemble (*e.g.*, in 40% water).

Nature of excimer emission

There are two types of excimers known.[13,17] One is called a 'dynamic excimer', in which there are no interactions between chromophores in the ground state. The excimer emission originates from dimer formation between an electronically excited monomer and a ground-state monomer. The second type is called a 'static' or 'pre-associated excimer' in which the chromophores interact with each other in the ground state, resulting in the formation of an excimer in the excited state.[16a,b] For **1** with heparin in 70% water, since the UV-Vis spectra show that the NDI molecules with heparin are aggregated (Fig. 1a), the fluorescence is expected to originate from a static excimer (Fig. 1b). However, the mostly monomeric nature of **1** with heparin in 40% water does not clearly reveal the nature of the excimer emission (Fig. 1d and e). To confirm the nature of the two excimers, excitation spectra were recorded at the monomer and excimer emission bands at 410 nm and 510 nm, respectively. For the 70% water sample with heparin, the excitation spectra collected at the excimer emission band (510 nm) show features similar to the aggregated form of NDI (Fig. 1f). On the other hand, the excitation spectra collected at 410 nm were very different and closely resembled the UV-Vis absorption spectra of monomeric **1** alone (Fig. 1f). Interestingly, the excitation spectra collected at 510 nm for the 40% sample with heparin also showed that the excimer emission indeed originates from the aggregated NDIs (Fig. S11). Thus, even though NDIs are mostly in the monomeric state in 40% water with heparin (Fig. 1d and e), the small fraction of **1** that binds to heparin (≈7%) leads to the formation of a static excimer.

More insight into the differences between these two solvent compositions came from NMR investigations. The ^{1}H NMR spectrum of **1** in 70% D_2O exhibited sharp NMR signals for the aromatic protons of the NDI core at δ 8.67 ppm. Upon addition of heparin, these aromatic signals showed a significant upfield shift ($\Delta\delta$ = 0.55 ppm) to δ 8.12 ppm, along with peak broadening (Fig. 2a and Fig. S12a for 99% water). This upfield shift and signal broadening of the aromatic protons indicate heparin binding-induced strong aromatic–aromatic interactions and self-assembly of **1**, which results in a pre-associated excimer. Contrarily, heparin binding in the 40% D_2O sample did not produce any significant difference in the chemical shift of the aromatic protons of NDI, and the peaks remained very sharp (Fig. 2b and Fig. S12b for 10% water). This confirms that the 40% sample of **1** with heparin remains mostly monomeric. Thus, the NMR analysis results are consistent with the UV-Vis data of Fig. 1a and d, showing that heparin induces aggregation of **1** only in 70% water and it is

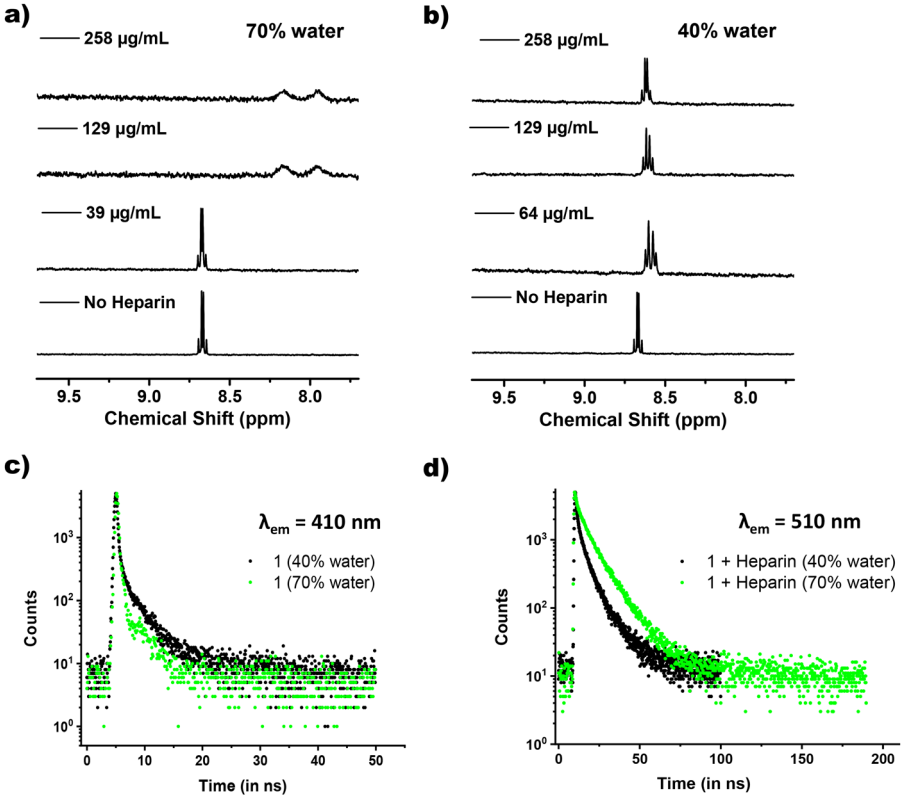

Fig. 2 (a) ^{1}H NMR spectra of **1** (0.5 mM) in 70% D_2O in acetonitrile solvent composition with different concentrations of heparin, showing upfield shifted and broadened bands due to π–π stacking interactions and aggregate formation; (b) ^{1}H NMR spectra of **1** (0.5 mM) in 40% D_2O in acetonitrile solvent composition with different concentrations of heparin showing no signal broadening; the TCSPC experiment showing the fluorescence decay profile of **1** without heparin (λ_{em} = 410 nm) in (c) and with heparin (λ_{em} = 510 nm) in (d) for 40% and 70% water in acetonitrile solvent compositions.

predominantly monomeric in 40% water. Additionally, cyclic voltammetry (CV) experiments were performed in these two solvent compositions to further support the heparin binding-induced changes (Fig. S13). As expected, the 40% sample with and without heparin showed very similar CV profiles, in line with the UV-Vis data in Fig. 1d. However, the 70% water sample with and without heparin showed very different CV profiles, with a significant shift in the reduction peak, in line with the heparin binding-induced changes observed in the absorption spectra in Fig. 1a.

To further confirm the nature of different emissions, time-correlated single photon counting experiments (TCSPC) were performed by exciting the sample with a 405 nm picosecond laser. For both the 40% and 70% water samples of **1** without heparin, the 410 nm emission exhibits a biexponential decay with a major contribution from a fast decay component of τ_1 = 0.18 ns (40% water sample) and τ_1 = 0.14 ns (70% water sample) (Fig. 2c, d and Table S1). Such sub-nanosecond decay profiles confirm the monomeric nature of the emission. Upon binding with heparin, the excimer emission at 510 nm also decays biexponentially. However, it exhibits a much slower fluorescence decay, and the lifetimes of the major component for the 40% and 70% water samples are τ_2 = 7.6 ns and τ_2 = 10.0 ns, respectively. This is similar to the reported lifetime of NDI excimers.[16a,18] Such long-lived fluorescent species could not have originated from simple aggregation and have been reported for excimer formation.[16b]

Heparin binding-induced supramolecular organization

To further investigate the supramolecular organization of **1** upon binding with heparin, we studied the morphological features using Transmission Electron Microscopy (TEM), Atomic Force Microscopy (AFM) and Confocal Laser Scanning Microscopy (CLSM). The air-dried sample of **1** with heparin in 70% water revealed the formation of well-defined nanofibers by TEM and AFM. For example, the TEM micrographs (Fig. 3a, b and S14) of **1** with heparin in 70% water showed the formation of supramolecular nanofibers. Furthermore, AFM micrographs also revealed a network of one-dimensional fibrillar nanostructures (Fig. 3c, d and S15).

We hypothesized an amphiphilic self-assembly of **1** with the hydrophobic tail embedded within the core and the hydrophilic part exposed to aqueous media along with two units of heparin bound on either side, as shown in Scheme 1. The molecular length of **1** was calculated to be around 2.2 nm (obtained from the geometry-optimized structure using ChemDraw 3D) and the width of the heparin monomer was estimated to be around 1 nm. Thus, the width of the self-

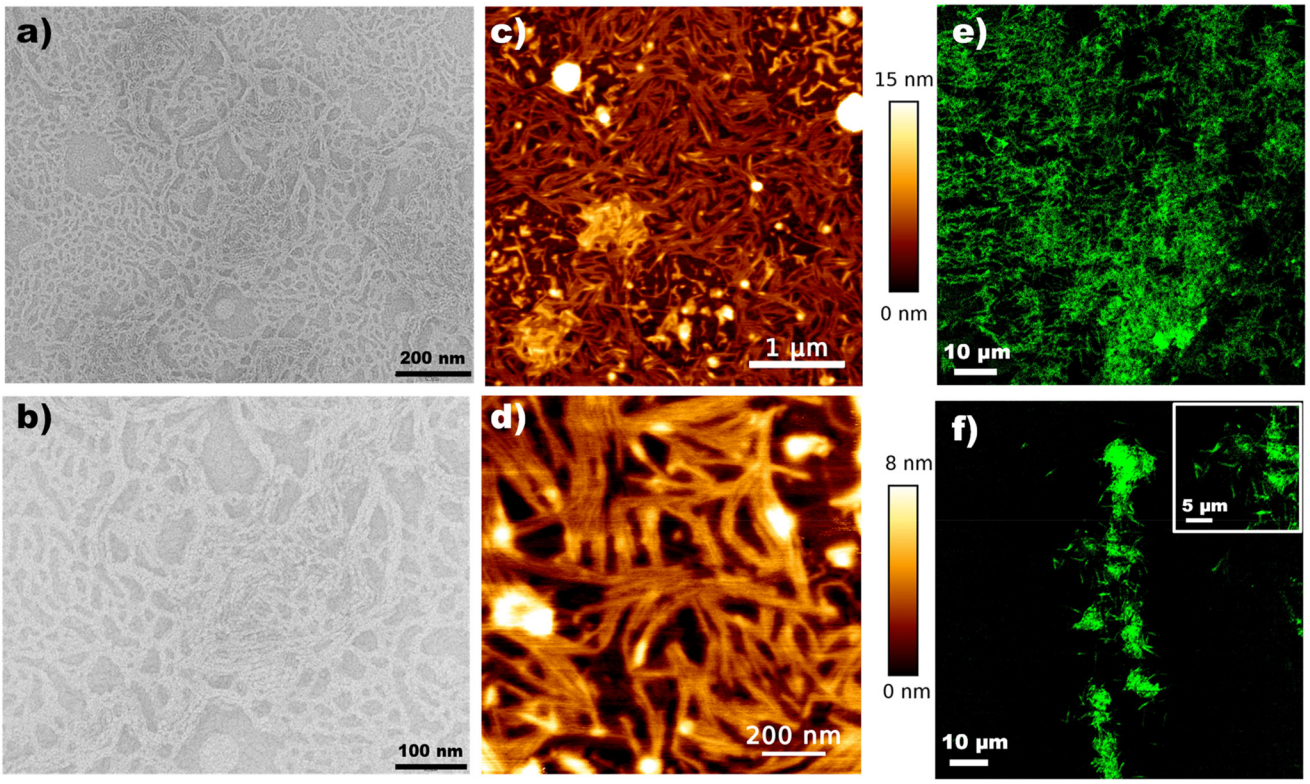

Fig. 3 (a and b) TEM and (c and d) AFM micrographs of surface-dried samples of **1** (50 μM) upon 12.9 μg ml^{-1} heparin binding in 70% H_2O in acetonitrile solvent composition. (e and f) Confocal Laser Scanning Microscopy (CLSM) images of a solution of **1** (200 μM) upon heparin binding, showing the formation of nanofibers in solution. Excitation at λ_{ex} = 405 nm and detection at the excimer band (λ_{em} = 500–700 nm) reveals intense green excimer emission along the nanofiber length, confirming that the aggregated state of **1** is fluorescent. The inset in (f) is a magnified image.

assembled structure shown in Scheme 1 is expected to be around 6 nm (Fig. S14). To confirm this molecular organization, dimensional analysis was performed on the micrographs in Fig. 3. From the TEM images, the nanofibers displayed lengths exceeding 1 μm and widths up to 22 nm (over 21 selected thin nanofibers). The width of the thinnest nanofiber was found to be 6.2 nm, which is close to the theoretical expectation from the organization shown in Scheme 1, reiterating the bilayer-like amphiphilic self-assembly. Additionally, the height of the nanostructure was obtained from the AFM micrographs. The height of some of the nanofibers was found to be below 2 nm, which is even shorter than the length of a single molecule of **1**. This rules out the formation of cylindrical micelles and thus supports the amphiphilic bilayer assembly in which the long axis of the nanofiber is the direction of π–π stacking, as shown in Scheme 1.

These techniques have clearly shown the formation of nanofibers, but the AFM and TEM imaging were performed on air-dried samples. Furthermore, they do not provide information about the fluorescent nature of the self-assembly. To confirm that these nanostructures also exist in the solution and that the structures are fluorescent, in-solution imaging was performed using CLSM. Traditionally, CLSM would require labelling the sample with a fluorescent dye. However, in our case, the self-assembly of **1** in the presence of heparin leads to aggregation-induced excimer emission, we could use the intrinsic fluorescence of the aggregates for CLSM imaging. The confocal micrographs clearly showed the formation of fluorescent fibrillar structures (Fig. 3e, f and S16). Of course, since confocal microscopy is an optical technique, it is limited in spatial resolution, and we could only observe large bundles of nanofibers. These images confirm two things about the self-assembled structures of **1** upon heparin binding: (a) the self-assembled nanofibers are indeed present in the solution and are not due to any drying-induced artifact and (b) the nanostructures are inherently fluorescent due to the formation of a static excimer.

Role of amphiphilic design and solvent composition

To demonstrate that the amphiphilic design is essential for heparin binding-induced excimer formation, we synthesized a bolaamphiphilic NDI derivative **2** (Schemes 1 and S2). This molecule has a positive charge on either side of the NDI aromatic core and lacks a hydrophobic alkyl chain. Molecule **2** is monomeric in water but self-assembles upon binding with heparin, as seen from the changes in the absorption spectra and the appearance of scattering at higher wavelengths in the UV-Vis absorption spectra (Fig. 4a and b). Thus, the absorption spectral changes are similar to those observed for the binding of heparin to the amphiphilic molecule **1**. In contrast, the fluo-

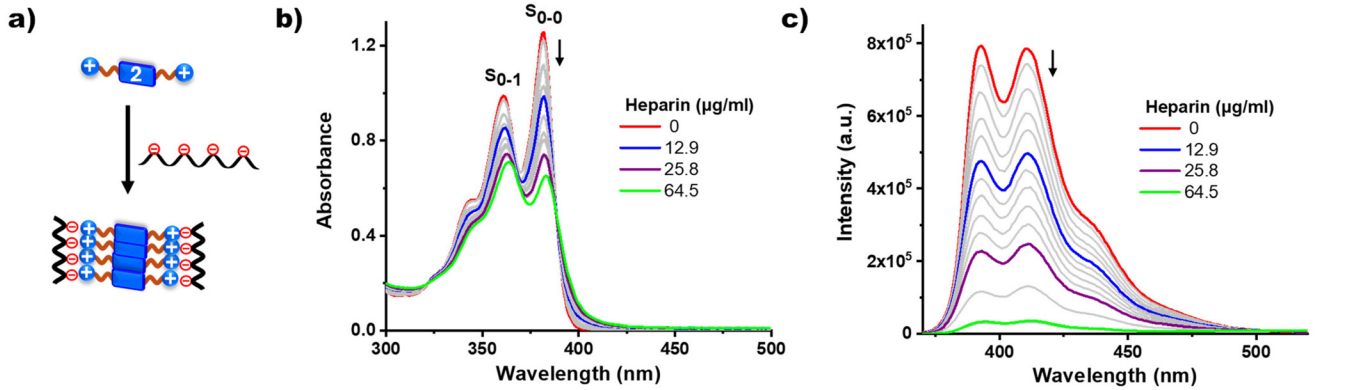

Fig. 4 (a) Schematic of heparin binding-induced self-assembly of bolaamphiphilic derivative **2**; (b) UV-Vis absorption and (c) emission spectra of **2** (50 μM) with varying concentrations of heparin in 99% water, showing a lack of excimer emission, as shown schematically in (a).

rescence spectra of **2** upon binding with heparin resulted in quenching of the monomeric emission without the emergence of any excimer emission (Fig. 4c). Thus, we clearly demonstrate the essential role of amphiphilic design for heparin binding-induced excimer emission. Furthermore, we also varied the carbon chain length from C_{10} in molecule **1** to C_{12} in molecule **3** (Scheme S2 and Fig. S17) of the amphiphilic design. The amphiphilic molecule **3** also behaved like **1** to display excimer emission and led to the formation of fluorescent nanostructures upon interaction with heparin. Thus, we showed that amphiphilic molecules display heparin-binding-assisted aggregation-induced green emission whereas the bolaamphiphile design (**2**) shows aggregation-induced quenching of monomeric emission.

Having confirmed that heparin binding resulted in excimer emission in **1** in various compositions of water in acetonitrile, we probed whether such observations were limited to these solvent mixtures. Thus, we performed experiments in water–

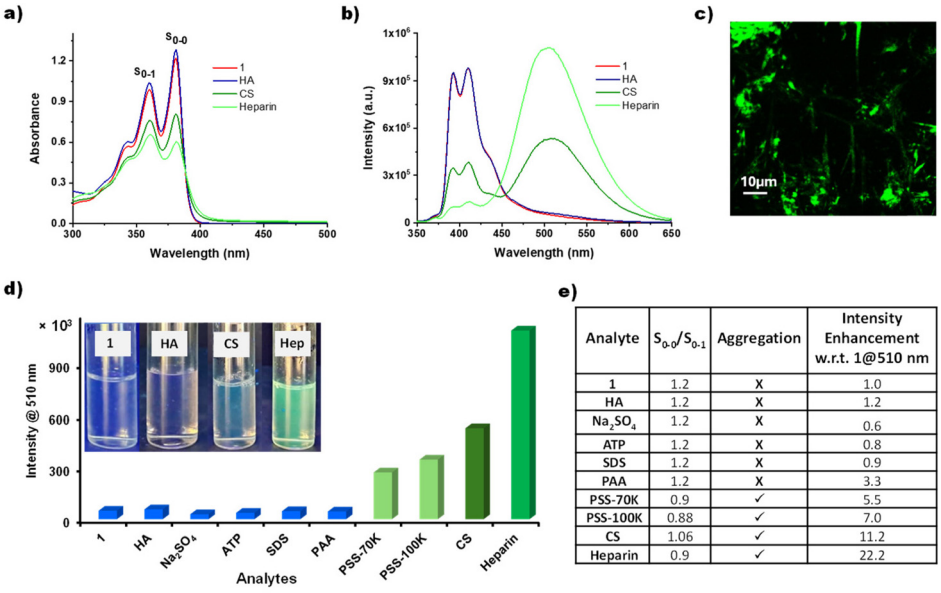

Analyte	S_{0-0}/S_{0-1}	Aggregation	Intensity Enhancement w.r.t. 1@510 nm
1	1.2	X	1.0
HA	1.2	X	1.2
Na_2SO_4	1.2	X	0.6
ATP	1.2	X	0.8
SDS	1.2	X	0.9
PAA	1.2	X	3.3
PSS-70K	0.9	✓	5.5
PSS-100K	0.88	✓	7.0
CS	1.06	✓	11.2
Heparin	0.9	✓	22.2

Fig. 5 (a) UV-Vis absorption and (b) emission spectra of **1** (50 μM) with addition of 2 molar equivalents (w.r.t. their monomers) of heparin and other GAGs in 70% H_2O in acetonitrile solvent composition; (c) CLSM image of the solution of **1** in the presence of CS, showing the formation of fluorescent nanofibers in solution. Excitation at λ_{ex} = 405 nm and detection at 500–700 nm; (d) bar graph of the fluorescence intensity of **1** at 510 nm upon addition of different analytes: hyaluronic acid (HA), Na_2SO_4, adenosine triphosphate (ATP), sodium dodecyl sulphate (SDS), polyacrylic acid (PAA), poly(sodium 4-styrenesulfonate) (PSS-70K), poly(sodium 4-styrenesulfonate) (PSS-100K), chondroitin sulphate (CS) and heparin (2 molar equivalents w.r.t. their monomers) [inset: photo of solutions of **1** in the presence of HA, CS and heparin in 70% H_2O under 365 nm UV light]. (e) A table representing the change in the ratio of UV-Vis absorbance peaks S_{0-0}/S_{0-1}, which clearly indicates the monomeric and aggregated nature of **1** in the presence of various analytes, and the corresponding fluorescence intensity enhancement at excimer emission (510 nm), plotted as a ratio of fluorescence intensity ($FI_{analyte}/FI_0$).

DMSO, water–DMF and water–methanol solvent compositions (Fig. S18). The detailed UV-Vis absorption and emission spectra of **1** in the presence of heparin in 70% aqueous solution of DMSO, DMF and methanol solvents confirmed that the excimer emission behavior was not limited to one solvent system. Furthermore, similar observation of excimer emission was made in other concentrations of **1**, ranging from 200 μM to 10 μM.

Sulphated glycosaminoglycan selective excimer response

Up to here, we have demonstrated that anionic heparin binds to cationic **1** to induce aggregation and excimer emission. To better understand the nature of the interaction between them, experiments were performed with other anionic glycosaminoglycans. Since heparin and CS both contain sulphated anions, while HA contains carboxylic acid-based anions, we investigated whether there are differences in fluorescence response in the presence of different GAGs. Thus, we investigated the spectroscopic response of **1** with CS in 70% water. Binding between CS and **1** also resulted in excimer emission at 510 nm, along with changes in the absorption spectra, and resulted in the formation of fluorescent nanofibers, similar to heparin binding, albeit with lower intensity (Fig. 5a–c). The binding constants of heparin and CS were estimated to be 9.4×10^4 M^{-1} and 7.7×10^4 M^{-1}, respectively, confirming slightly higher affinity for heparin compared to CS (Fig. S19). Interestingly, addition of HA to **1** did not result in excimer formation nor any change in the UV-Vis absorption spectra (Fig. 5a and S20). Any unintended effects of pH variation were ruled out by performing heparin and HA-binding experiments at the same pH (Fig. S21a–c). These data clearly confirm that sulphated anions, and not carboxylic acid anions, interact specifically with cationic **1** to induce excimer emission. Such observations demonstrate that the fluorescence response of **1** can distinguish sulphated from carboxylated glycosaminoglycans (heparin and CS from HA) to produce a differential fluorescence response.

To further probe the essential role of bio-polymeric sugars in producing aggregation and fluorescence response in **1**, several other anions were tested (Fig. 5d, e and S20a–c). For example, sodium sulphate did not produce any spectroscopic changes. Instead, polystyrene sulfonates (PSS) produced significant UV-Vis changes, to an extent greater than that observed for heparin binding. This indicates that PSS binding caused significant aggregation of **1**, even more than that induced by heparin binding. However, it produced very weak excimer emission (nearly 300% lower compared to the **1** + heparin sample). Furthermore, monovalent sulfonate anions also did not bind to **1**, indicating the essential role of multivalency (Fig. S22). Similarly, polyacrylic acid showed no excimeric emission, whereas the sodium salt of polyacrylic acid yielded very weak excimer emission. Taken together, these results demonstrate that the biopolymeric sugar and sulphated GAG scaffold plays a crucial role in controlling the supramolecular organization of **1**, resulting in the formation of high-intensity excimer emission (Fig. 5b).

Conclusions

In conclusion, we demonstrate a heparin binding-induced supramolecular polymerization of cationic NDI amphiphiles, resulting in the formation of fluorescent nanofibers exhibiting strong excimer emission. Selective binding of sulphated GAGs like heparin and CS results in the self-assembly of NDIs, whereas the non-sulphated GAG (HA) does not interact. Our detailed investigation showed that the amphiphilic molecular architecture was essential for achieving heparin binding-induced excimer emission, as shown by a structural analogue lacking hydrophobic character. Additionally, we showed that the fluorescence response can distinguish biological sulphated derivatives from the synthetic ones. Thus, we present a unique example of (a) sulphated GAG-directed formation of fluorescent nanostructures and (b) selective induction of supramolecular organization and fluorescence response in these NDIs by biopolymeric sulphates. This work highlights a versatile strategy to translate biomolecular recognition into supramolecular organization with desirable photophysical response, paving the way for the design of GAG-directed formation of fluorescent materials. Future experiments in the lab are exploring the compatibility of this design in biological milieus for potential biosensing and imaging applications.

Author contributions

MK and PS conceived the idea; PS and EFPL performed the synthesis. PS conducted most of the spectroscopic and microscopic studies. BCN and AC designed and performed AFM, whereas SG performed CLSM imaging. PR and XC designed and executed the CV measurements, whereas BL performed and analysed the TCSPC experiments. PS and MK wrote the manuscript. All the authors read and commented on the manuscript.

Conflicts of interest

There are no conflicts to declare.

Data availability

Supplementary information: detailed synthetic methods, characterization details and other supporting figures. See DOI: https://doi.org/10.1039/d5nr04833h.

Additionally, the raw data can be made available upon reasonable request.

Acknowledgements

MK acknowledges funding from the Ramon y Cajal fellowship (RYC2021-035016-I) from the Spanish Ministry of Science and Innovation (MICIU/AEI/10.13039/501100011033) and the European Union NextGenerationEU/PRTR. Additional funding

was provided by the Proyectos de Generación de Conocimiento grant (PID2021- 126244NA-I00) from the Spanish Ministry of Science and Innovation. MK and BL thank the Agencia Estatal de Investigación for the María de Maeztu CEX2021-001202-M. The authors also acknowledge support from the "la Caixa" Foundation, CaixaResearch Health 2024 program under the grant agreement LCF/PR/HR24/52440012. BL thanks the European Research Council (ERC) for an ERC-StG (Grant Agreement No. 101076014).

References

1 (*a*) T. Aida, E. W. Meijer and S. I. Stupp, *Science*, 2012, **335**, 813–817; (*b*) Z. Chen, A. Lohr, C. R. Saha-Moller and F. Wurthner, *Chem. Soc. Rev.*, 2009, **38**, 564–584; (*c*) S. S. Babu, V. K. Praveen and A. Ajayaghosh, *Chem. Rev.*, 2014, **114**, 1973–2129; (*d*) F. García, R. Gómez and L. Sánchez, *Chem. Soc. Rev.*, 2023, **52**, 7524–7548.

2 (*a*) A. Mishra, S. Dhiman and S. J. George, *Angew. Chem., Int. Ed.*, 2021, **60**, 2740–2756; (*b*) X. Ma and H. Tian, *Acc. Chem. Res.*, 2014, **47**, 1971–1981.

3 (*a*) P. A. Korevaar, S. J. George, A. J. Markvoort, M. M. Smulders, P. A. Hilbers, A. P. Schenning, T. F. De Greef and E. W. Meijer, *Nature*, 2012, **481**, 492–496; (*b*) K. Shimomura, T. Ikai, S. Kanoh, E. Yashima and K. Maeda, *Nat. Chem.*, 2014, **6**, 429–434; (*c*) F. Riobe, A. P. Schenning and D. B. Amabilino, *Org. Biomol. Chem.*, 2012, **10**, 9152–9157; (*d*) A. Mammana, A. D'Urso, R. Lauceri and R. Purrello, *J. Am. Chem. Soc.*, 2007, **129**, 8062–8063; (*e*) K. Toyofuku, M. A. Alam, A. Tsuda, N. Fujita, S. Sakamoto, K. Yamaguchi and T. Aida, *Angew. Chem., Int. Ed.*, 2007, **46**, 6476–6480.

4 (*a*) J. Deng and A. Walther, *Adv. Mater.*, 2020, **32**, e2002629; (*b*) Y. Bai, Q. Luo and J. Liu, *Chem. Soc. Rev.*, 2016, **45**, 2756–2767; (*c*) Y. Wang, J. Nie, W. Fang, L. Yang, Q. Hu, Z. Wang, J. Z. Sun and B. Z. Tang, *Chem. Rev.*, 2020, **120**, 4534–4577; (*d*) M. Kumar, N. Jonnalagadda and S. J. George, *Chem. Commun.*, 2012, **48**, 10948–10950.

5 (*a*) S. Li, H. Deng, Y. Fan and Y. Ding, *Dyes Pigm.*, 2025, **242**, 113000; (*b*) Y. Li, Y. Zhang, X. Liu, B. Dong, P. Xu and B. Song, *Langmuir*, 2024, **40**, 26626–26632; (*c*) L. Shao, H. Yu, J. Song, S. Liu and G. Li, *ChemBioChem*, 2023, **24**, e202200652; (*d*) L. Fan, D. Jia, W. Zhang and Y. Ding, *Analyst*, 2020, **145**, 7809–7824; (*e*) D. Kim, U. Lee, J. Bouffard and Y. Kim, *Adv. Opt. Mater.*, 2020, **8**, 1902161; (*f*) L. J. Chen, Y. Y. Ren, N. W. Wu, B. Sun, J. Q. Ma, L. Zhang, H. Tan, M. Liu, X. Li and H. B. Yang, *J. Am. Chem. Soc.*, 2015, **137**, 11725–11735.

6 (*a*) S. S. Lee, B. J. Huang, S. R. Kaltz, S. Sur, C. J. Newcomb, S. R. Stock, R. N. Shah and S. I. Stupp, *Biomaterials*, 2013, **34**, 452–459; (*b*) P. Sharma and S. Roy, *Nanoscale*, 2023, **15**, 7537–7558; (*c*) V. M. P. Vieira, A. C. Lima, M. de Jong and D. K. Smith, *Chem. – Eur. J.*, 2018, **24**, 15112–15118.

7 (*a*) Q. Dai, W. Liu, X. Zhuang, J. Wu, H. Zhang and P. Wang, *Anal. Chem.*, 2011, **83**, 6559–6564; (*b*) S. K. Bhaumik and S. Banerjee, *Analyst*, 2021, **146**, 2194–2202; (*c*) J. Zheng, T. Ye, J. Chen, L. Xu, X. Ji, C. Yang and Z. He, *Biosens. Bioelectron.*, 2017, **90**, 245–250; (*d*) L. Zeng, P. Wang, H. Zhang, X. Zhuang, Q. Dai and W. Liu, *Org. Lett.*, 2009, **11**, 4294–4297; (*e*) L. Fan, D. Jia, W. Zhang and Y. Ding, *Analyst*, 2021, **145**, 7809–7824; (*f*) A. K. Ghosh, P. Choudhury and P. K. Das, *Langmuir*, 2019, **35**, 15180–15191; (*g*) J. Ma, R. Sun, K. Xia, Q. Xia, Y. Liu and X. Zhang, *Chem. Rev.*, 2024, **124**, 1738–1861; (*h*) M. Babazadeh-Mamaqani, D. Razzaghi, H. Roghani-Mamaqani, A. Babaie, M. Rezaei, R. Hoogenboom and M. Salami-Kalajahi, *Prog. Mater. Sci.*, 2024, **146**, 101312; (*i*) W. Liu, Q. Liu, D. Wang and B. Z. Tang, *ACS Nano*, 2024, **18**, 27206–27229.

8 (*a*) S. K. Bhaumik, Y. S. Patra and S. Banerjee, *Chem. Commun.*, 2020, **56**, 9541–9544; (*b*) R. Biswas and S. Banerjee, *Biomacromolecules*, 2023, **24**, 766–774.

9 (*a*) W. Ji, X. Zhang, J. Zhao, Y. Gao, W. Song and Y. Ozaki, *Analyst*, 2018, **143**, 1899–1905; (*b*) G. H. Aryal, G. R. Rana, F. Guo, K. W. Hunter and L. Huang, *Chem. Commun.*, 2020, **56**, 13437–13440; (*c*) J. Li, J. Xu, W. Guo, W. Zhong, Q. Li, L. Tan and L. Shang, *Sens. Actuators, B*, 2020, **305**, 127422.

10 (*a*) F. Wurthner, C. R. Saha-Moller, B. Fimmel, S. Ogi, P. Leowanawat and D. Schmidt, *Chem. Rev.*, 2016, **116**, 962–1052; (*b*) S. V. Bhosale, M. Al Kobaisi, R. W. Jadhav, P. P. Morajkar, L. A. Jones and S. George, *Chem. Soc. Rev.*, 2021, **50**, 9845–9998; (*c*) M. Kumar, N. L. Ing, V. Narang, N. K. Wijerathne, A. I. Hochbaum and R. V. Ulijn, *Nat. Chem.*, 2018, **10**, 696–703; (*d*) N. Sakai, J. Mareda, E. Vauthey and S. Matile, *Chem. Commun.*, 2010, **46**, 4225–4237; (*e*) A. Sikder, S. Chakraborty, P. Rajdev, P. Dey and S. Ghosh, *Acc. Chem. Res.*, 2021, **54**, 2670–2682.

11 X. Liang, H. Nie, C. Yang, Z. Wang, J. Bai and H. Yan, *J. Mol. Liq.*, 2021, **343**, 117585.

12 (*a*) S. Noel, B. Liberelle, L. Robitaille and G. De Crescenzo, *Bioconjugate Chem.*, 2011, **22**, 1690–1699; (*b*) P. Sharma, A. Venugopal, C. M. Verdi, M. S. Roger, A. Calo and M. Kumar, *J. Mater. Chem. B*, 2024, **12**, 7292–7297; (*c*) M. Kumar, J. Son, R. H. Huang, D. Sementa, M. Lee, S. O'Brien and R. V. Ulijn, *ACS Nano*, 2020, **14**, 15056–15063; (*d*) Z. Huang, C. Jia, B. Wu, S. Jansone-Popova, C. A. Seipp and R. Custelcean, *Chem. Commun.*, 2019, **55**, 1714–1717.

13 J. Mei, N. L. Leung, R. T. Kwok, J. W. Lam and B. Z. Tang, *Chem. Rev.*, 2015, **115**, 11718–11940.

14 (*a*) Z.-R. Han, Y.-F. Wang, X. Liu, J.-D. Wu, H. Cao, X. Zhao, W.-G. Chai and G.-L. Yu, *Chin. J. Anal. Chem.*, 2011, **39**, 1352–1357; (*b*) A. Tuzikov, N. Shilova, T. Ovchinnikova, A. Nokel, O. Patova, Y. Knirel, T. Chernova, T. Gorshkova and N. Bovin, *Polysaccharides*, 2024, **5**, 1–15.

15 H. Shao and J. R. Parquette, *Chem. Commun.*, 2010, **46**, 4285–4287.

16 (*a*) S. A. Boer, R. P. Cox, M. J. Beards, H. Wang, W. A. Donald, T. D. M. Bell and D. R. Turner, *Chem. Commun.*, 2019, **55**, 663–666; (*b*) M. Kumar, O. A. Ushie and S. J. George, *Chem. – Eur. J.*, 2014, **20**, 5141–5148; (*c*) D. A. Shejul, S. M. Wagalgave, R. W. Jadhav,

M. A. Kobaisi, D. D. La, L. A. Jones, R. S. Bhosale, S. V. Bhosale and S. V. Bhosale, *New J. Chem.*, 2020, **44**, 1615–1623.

17 (*a*) V. Kumar, B. Sk, S. Kundu and A. Patra, *J. Mater. Chem. C*, 2018, **6**, 12086–12094; (*b*) A. Ghosh, A. Sengupta, A. Chattopadhyay and D. Das, *Chem. Commun.*, 2015, **51**, 11455–11458; (*c*) C. Li, X. Xie, M. Li, H. Wang, X. Cheng, J. Zhang, Q. Li, J. Li, X. Zuo, C. Fan and J. Shen, *J. Am. Chem. Soc.*, 2024, **146**, 18948–18957.

18 M. Kumar and S. J. George, *Nanoscale*, 2011, **3**, 2130–2133.